2008

Compressive Properties of Trabecular Bone in the Distal Femur

Travis A. Burgers

Jim Mason

Glen Niebur

Heidi L. Ploeg

Compressive properties of trabecular bone in the distal femur

Travis A. Burgers[a], Jim Mason[b], Glen Niebur[c], Heidi L. Ploeg[a,*]

[a]Mechanical Engineering Department, University of Wisconsin, Madison, WI, USA

[b]Research Laboratory, Zimmer Inc., Warsaw, IN, USA

[c]Aerospace and Mechanical Engineering Department, University of Notre Dame, South Bend, IN, USA

*Corresponding author. Tel.: +1608 262 2690; fax: +1608 265 2316; E-mail address: ploeg@engr.wisc.edu (H.L. Ploeg).

Abstract

Early loosening and implant migration are two problems that lead to failures in cementless (press-fit) femoral knee components of total knee replacements. To begin to address these early failures, this study determined the anterior–posterior mechanical properties from four locations in the human distal femur. Thirty-three cylindrical specimens were removed perpendicular to the press-fit surface after the surgical cuts on 10 human cadaveric femurs (age 71.5 ± 14.2 years) had been made. Compression testing was performed that utilized methods to reduce the effects of end-artifacts. The bone mineral apparent density (BMAD), apparent modulus of elasticity, yield and ultimate stress, and yield and ultimate strain were measured for 28 cylindrical specimens. The apparent modulus, yield and ultimate stress, and yield and ultimate strain each significantly differed ($p<0.05$) in the superior and inferior locations. Linear and power law relationships between superior and inferior mechanical properties and BMAD were determined. The inferior apparent modulus and stresses were higher than those in the superior locations. These results show that the press-fit fixation characteristics of the femoral knee component differ on the anterior shield and posterior condyles. This information will be useful in the assignment of mechanical properties in finite element models for further investigations of femoral knee components. The property–density relations also have applications for implant design and preoperative assessment of bone strength using clinically available tools.

Keywords: Cancellous bone; Distal femur; Apparent modulus; Bone mineral apparent density; Femoral knee components

Notation

ANCOVA – analysis of covariance

AP – anterior-posterior

BMAD – bone mineral apparent density

DXA – Dual energy X-ray absorptiometery

E – apparent modulus of elasticity

FE – Finite element

ML – medial-lateral

p – probability of obtaining a result at least as extreme as that obtained

QCT – quantitative computed tomography

R^2 – coefficient of determination

SI – superior-inferior

TKA – total knee arthroplastic surgery

ε_{yield} – yield strain

$\varepsilon_{ultimate}$ – ultimate strain

μ-CT – micro computed tomography

σ_{yield} – yield stress

$\sigma_{ultimate}$ – ultimate stress

1. Introduction

The fixation between the distal femur and a cementless femoral knee component is of concern during a total knee arthroplasty (TKA). The fixation of cementless implants is initially caused by a press-fit between the bone and the implant. Over time, the cementless implant utilizes a porous coating that encourages osseointegration and supplements the press-fit fixation (Pilliar, 2005).

Loosening is one of the most common causes of failure of a TKA (Fehring and McAvoy, 1996), but it is difficult to diagnose (Reckling et al., 1977; Insall et al., 1983). Fehring et al. (2001) detailed the early failures of cementless TKAs. Their study included 440 patients who required TKA revision surgery within 5 years of the initial surgery between 1986 and 1999. Of the patients who underwent revision surgery, 27% of the cases were due to implant migration and 3% were a result of loosening. Fehring and Griffin (1998) performed 268 TKA revision surgeries over a 10 year period. They found that 23.5% of the patients (63 total: 36 cemented and 27 cementless) required a revision for loosening. Sharkey et al. (2002) recorded the failure mechanisms of TKA revision surgeries between 1997 and 2000. They divided their 203 subjects into an early (<2 years after surgery) and a late (>2 years) failure group. The revision surgeries were performed at an average of 1.1 and 7 years after the initial surgery in the early and late failure groups, respectively. They found that of those with revision surgery, loosening and migration accounted for 16.9% and 21.2%, respectively, of the revisions in early failures and 34.4% and 22.2%, respectively, of the late failures.

Finite element (FE) models have been used to analyze the bone–implant composite since the 1970s (Huiskes and Chao, 1983; Verdonschot et al., 1993). Recently, these FE models have been created from quantitative computed tomography (QCT) scan data (Perillo-Marcone et al., 2004; Shultz et al., 2006). The mechanical properties, however, of the bone are often not known and therefore material testing of the bone to be modeled is required. The mechanical properties of cancellous bone depend on both the density and the architecture. QCT data can be used to create anatomically accurate bone models with nonhomogeneous density representations (Keyak et al., 1990; Taylor et al., 2002). The mechanical properties of the bone can be assigned from empirical relationships between properties and QCT density (McBroom et al., 1985; Esses et al., 1989; Hvid et al., 1989; Lotz et al., 1990; Ciarelli et al., 1991; Rho et al., 1995). Dual energy X-ray absorptiometry (DXA), a common clinical tool, can be used to measure bone mineral density as an area density measurement; however, differences in sample thickness produce considerable disparities in the results (Nielsen, 2000). Bone mineral apparent density (BMAD) is the bone mineral content from DXA divided by the volume. It is proportional to apparent density and is a preferred measure over DXA areal

density because it is volumetric (Carter et al., 1992). Volumetric CT density is a preferred method for generating FE models for strength analyses as was confirmed by Cody et al. (1999) in a study of the femoral neck.

Previous studies on the mechanical properties of cancellous bone in the human distal femur have not fully investigated properties relevant to the press-fit of a distal femoral component. Du et al. (2006) performed compression, tension, torsion, shear, bending, and impact testing on the distal femur to quantify properties along the longitudinal axis of the bone. Rho et al. (1995) also studied the distal femur by measuring the modulus of elasticity in the superior–inferior (SI), medial–lateral (ML), and anterior–posterior (AP) directions using ultrasonic techniques. They found good linear correlations between bone density from QCT scans and the modulus in the AP direction. The differences between a linear and a power law regression were small in the normal physiological range. Ciarelli et al. (1991) also found linear and power law relationships between modulus and density in the distal femur. Further testing is needed in the AP direction since Rho et al. used ultrasonic rather than mechanical testing, Ciarelli et al. and Du et al. tested specimens that were subject to end effect errors (Keaveny et al., 1997) and Du et al. tested in the longitudinal direction of the bone.

Cancellous bone has orthotropic mechanical properties because of the directional structure of its trabecular microstructure. The principal material directions are aligned with the principal direction of the structural architecture (Zysset et al., 1998). In general, it is important to know trabecular orientation a priori when performing mechanical testing because the results are difficult to interpret otherwise (Turner and Cowin, 1988). But the trabecular orientation is not required to be known if the cancellous bone is tested in a predetermined direction of interest. It is assumed that the press-fit in the femoral component of the TKA applies a normal force to the bone–implant contact surface primarily in the AP direction (the normals to the anterior shield and condyles are 51 and 31 from the AP direction, respectively); thus, the AP direction is of interest in this application. The data available from the literature are insufficient for a study of a press-fit femoral knee component because most studies on cancellous bone have been performed either at different anatomical sites or the ones performed on the distal femur have been in the SI direction. A study reporting cancellous properties of cores aligned in the principal orientation would be difficult to relate to the press-fit application because the bone is not primarily loaded along the principal material axis. Additionally, this principal axis varies throughout the region of the implant. Thus, the purpose of this study was to determine the compressive mechanical properties of the cancellous bone of the human distal femur in the AP direction. The specific aims were to measure the modulus and strength of trabecular bone at four locations in the distal femur in the AP direction and determine the dependence of these properties on measured bone mineral density.

2. Materials and methods

Thirty-three cylindrical human cancellous bone specimens were obtained from eight cadavers (10 femurs; 4 male, 4 female; mean age 71.5 ± 14.2 years, age range 45–92) via the Uniform Anatomical Gift Act. Twenty-eight specimens were used in this study. The other five specimens were excluded because of transverse holes from surgery and testing failures. The femurs were received with the soft tissue removed.

Each had been wrapped in a saline-saturated gauze, sealed in an airtight plastic bag, and frozen to -20 °C. Each femur was thawed at room temperature and a surgical arthroplasty was performed. The cuts were made using the surgical instrument set and procedure designed for the Zimmer NexGens (Zimmer, Inc., Warsaw, IN) femoral knee component. Surgeries were performed so that cancellous specimens could be

harvested in a repeatable manner; that is, the specimens were oriented perpendicularly to the surgical cuts and therefore the surfaces of the implant.

Two transverse slices were removed from each femur after the surgery. Each slice was approximately 25 mm thick. These slices were labeled superior and inferior. The slices were specifically located to acquire bone specimens from the primary regions of interest: the posterior surface in contact with the implant's posterior condyles and the anterior surface in contact with the implant's anterior shield. The inferior slice contained the two surfaces in contact with the posterior condyles. The superior slice contained the anterior surface of the bone in contact with the anterior shield. This is shown in Figure 1.

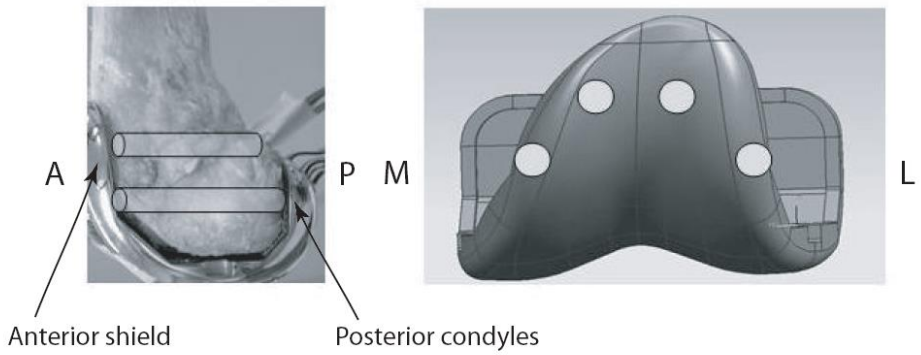

Figure 1: Cores were taken at two locations in the SI direction corresponding to the anterior shield, and the intercondylar region of the implant (left). Cores were taken from both medial and lateral locations in each SI slice (right).

Each slice was secured in a bone vice and was submerged in water. Twenty-eight cylindrical specimens, roughly 8.1 mm in diameter by 35 mm long, were prepared using an 8.1 mm diameter diamond-tipped coring bit (Starlite Industries, Inc., Rosemont, PA) in a drill press (Delta Shopmaster DP200, Delta Machinery, Jackson, TN). The drill directions of the superior and inferior specimens were perpendicular to the anterior and posterior surfaces, respectively. Therefore, the longitudinal axis of each cylinder was approximately in the AP direction. (The surgical cuts deviate slightly from the SI axis. Thus, the superior and inferior specimens were rotated 5° and 3°, respectively, in the sagittal plane from the AP direction due to the angle of the anterior shield and posterior condyles.) A specimen was harvested from approximately the center of each posterior condyle surface. The anterior specimens were harvested approximately 5–10 mm both medially and laterally from the center line of the medullary canal (see Figure 1). A bone rongeur and a scalpel were used to cut the specimens into right cylinders and to remove any cortical bone.

The length and diameter of each specimen were measured using a vernier caliper (Fowler, Newton, MA). The specimens were scanned using DXA (Lunar Corporation, Madison, WI). The specimens were oriented so the X-rays propagated the length of the cylindrical axis. The DXA software calculated area bone mineral density (in g/cm^2) by integrating through the length of the cylinder. BMAD (in g/cm^3) was calculated by dividing the area bone mineral density by the integration distance, i.e. the length of the specimen (Carter et al., 1992). BMAD from DXA was used in this study so that bone strength and modulus in the distal femur could be estimated using a common, clinically available tool, namely DXA.

Each specimen was fixed with adhesive in stainless steel endcaps for compression testing (Keaveny et al., 1997). The end 8–10 mm of each specimen was sprayed with water using a Waterpik (Newport Beach, CA) to remove marrow. Then one end was submerged in ethyl alcohol for at least 1 min and dried using compressed air. Loctite 401 (Rocky Hill, CT) was applied to the stainless steel endcap and to the specimen, and a length of approximately 8 mm of the specimen was embedded in the endcap using a twisting motion to distribute the adhesive around the circumference of the bone specimen. The effective gauge length was calculated by adding the length between the endcaps and one-half the length of the core inside each endcap. This effective gauge length was experimentally determined by Keaveny et al. (1997). Each specimen was sealed in an airtight bag and placed in a -20 °C freezer within 15 min of being fixed in the endcaps. The specimens were frozen overnight while the adhesive fully cured.

The specimens were tested in compression using an Enduratec universal testing machine (Smart Test-AT, model number 2800-650, Bose Corporation, Minnetonka, MN), as shown in Figure 2. Load was measured through the Enduratec load cell (maximum load 12.5 kN) and the relative displacement between the endcaps was measured using an extensometer (Epsilon Technologies, model 3542, Jackson, WY). The specimens were tested to failure at a strain rate of 0.005 s^{-1} (Keaveny et al., 1997). Each test was continued past failure to emphasize the failure surface and the failure mechanism was recorded.

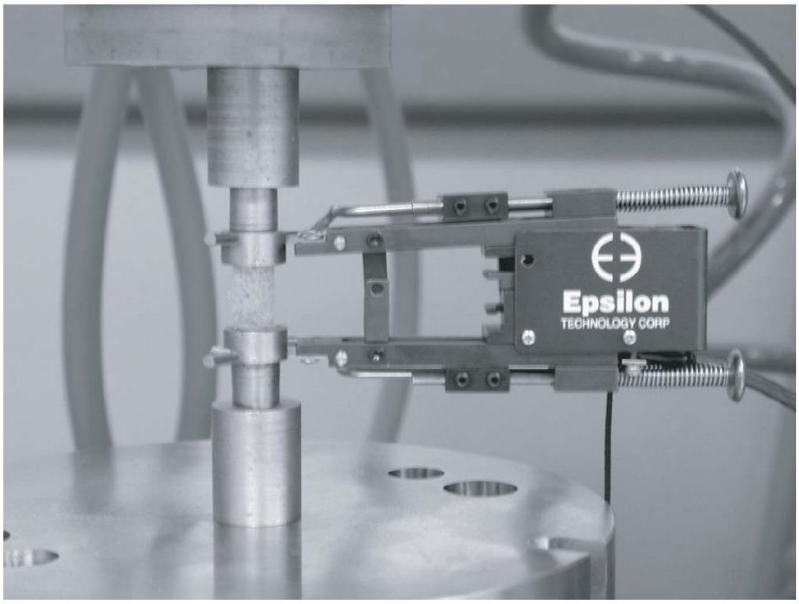

Figure 2: Compression testing setup. Cores were fixed in endcaps to eliminate end effects. Force was measured by the universal testing machine and displacement was measured using an extensometer with data acquisition software.

Stress and strain were calculated assuming continuum mechanics and Hooke's Law. The apparent modulus of elasticity (macroscopic) for each specimen was determined from the slope of the curve between 20% and 85% of the ultimate stress. A similar standardized method was previously used by Keaveny et al. (1994a) to calculate the modulus. The yield stress was determined from the 0.2% offset method and the ultimate stress was the maximum stress from the compression test. The yield strain and ultimate strain corresponded to the yield and ultimate stresses.

An unbalanced two-way analysis of covariance (ANCOVA) was performed on the data (Minitab R14.2, Minitab, Inc., State College, PA) to determine if coring location had a significant effect on the mechanical properties. The SI location was used as the treatment and the ML location was used as the block. BMAD was used as the covariance for apparent modulus of elasticity, yield and ultimate stress, and yield and ultimate strain. Failure mode was also considered as a covariance term for the stresses and strains. A regression was then performed on both the data and the log transform of the data. A linear model was chosen assuming axial deformation. A power law model was chosen because cellular structures have a power law relationship between density and elastic modulus (Gibson and Ashby, 1997).

3. Results

A representative stress–strain curve for the compression testing is shown in Figure 3. The average coefficient of determination (R^2) of the 28 specimens was 0.988 ± 0.009.

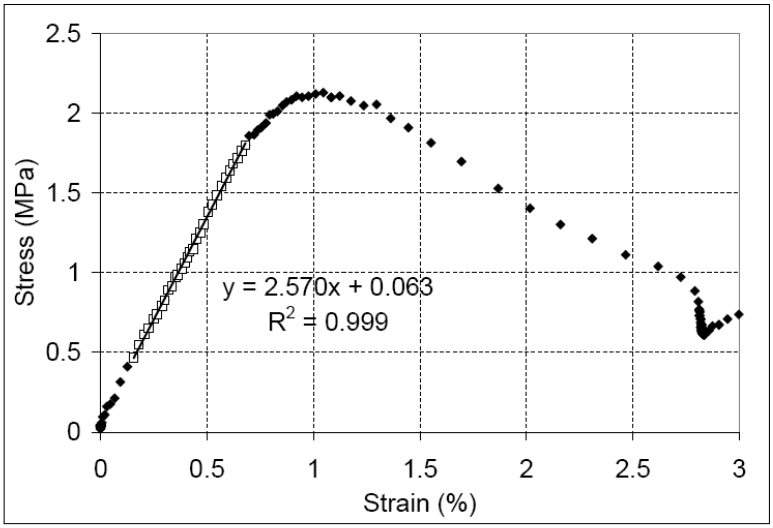

Figure 3: A representative stress-strain curve. The open squares shows data points in the region (20 to 85% of ultimate stress) used to calculate the apparent modulus of elasticity. The coefficient of determination of the twenty-eight specimens averaged 0.988.

The apparent modulus of elasticity, yield stress, and yield strain were significantly correlated with BMAD (Figure 4). The regressions were significantly different between the superior and inferior locations ($p<0.05$, ANCOVA). The ultimate stress and strain were also significantly correlated with BMAD, and the regressions differed between the superior and inferior locations ($p<0.05$). The medial and lateral locations were not significantly different for any of the regressions.

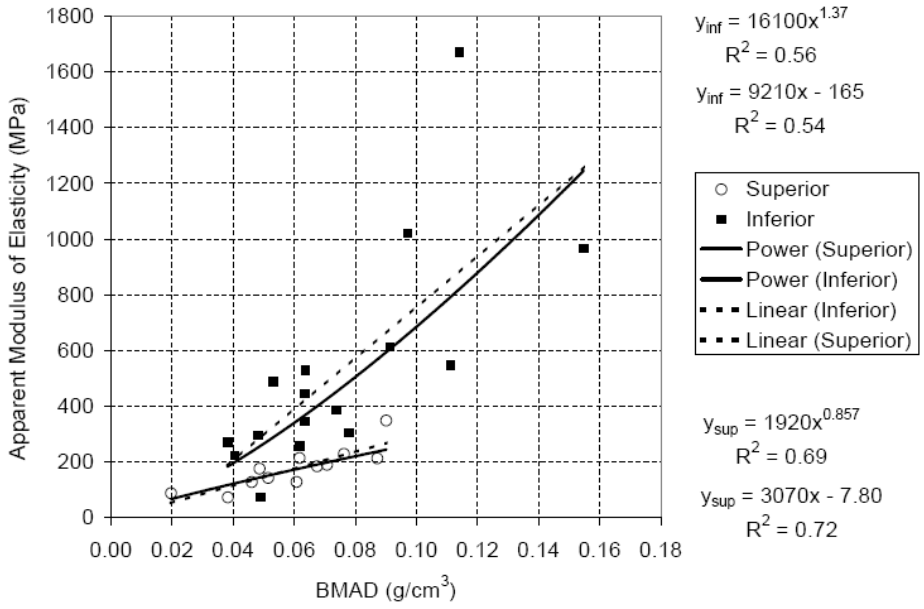

Figure 4a: Apparent modulus of elasticity versus bone mineral apparent density. Each of the linear and power coefficients was significantly different for the superior and inferior regions, except the linear constant, which was not significantly different from zero.

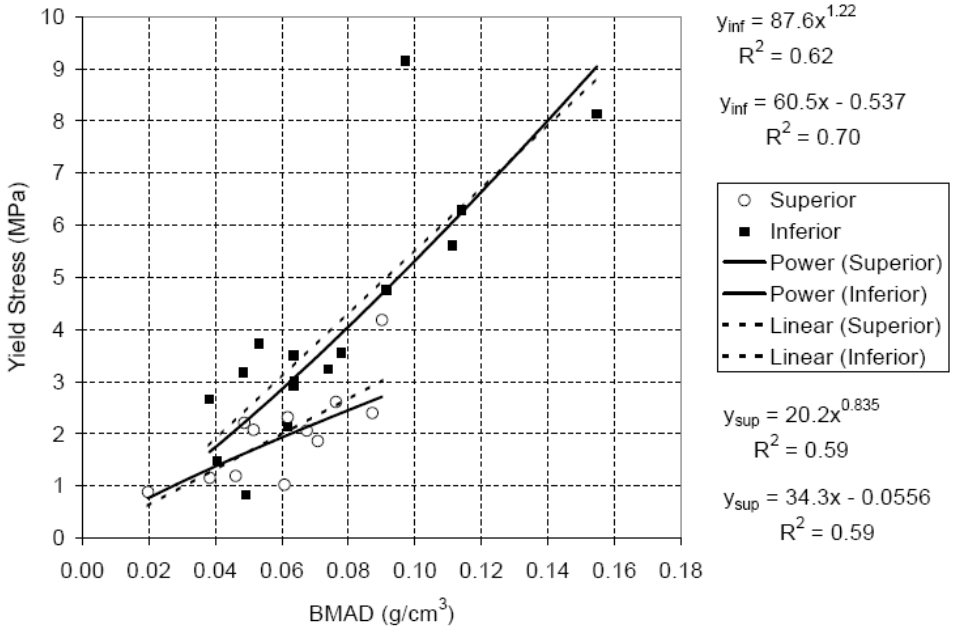

Figure 4b: Yield stress versus bone mineral apparent density. Each of the linear and power coefficients was significantly different for the superior and inferior regions, except the linear constant, which was not significantly different from zero.

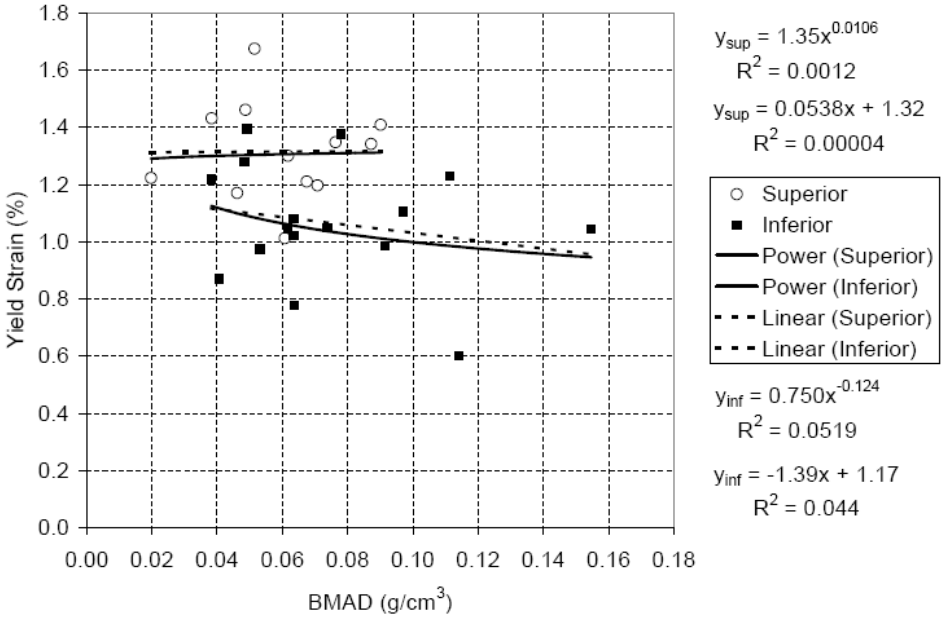

Figure 4c: Yield strain versus bone mineral apparent density. The multiplicative coefficient in the power equation and the constant in the linear equation were significantly different for the superior and inferior regions. The power coefficient in the power equation and the multiplicative coefficient in the linear equation were not significantly different from zero. This means each equation provides a constant yield strain that does not vary with density.

The mean BMAD, apparent modulus of elasticity, yield stress, ultimate stress, yield strain, and ultimate strain are shown for each location, the superior and inferior locations, and the pooled data in Figure 5. The inferior location had a higher apparent modulus, yield stress, and ultimate stress but had lower yield and ultimate strains than the superior location. Tables 1 and 2 show the power law and linear relationships, respectively, between the properties and the BMAD. The yield stress was linearly correlated to the modulus, consistent with the yield strains being approximately constant for each site.

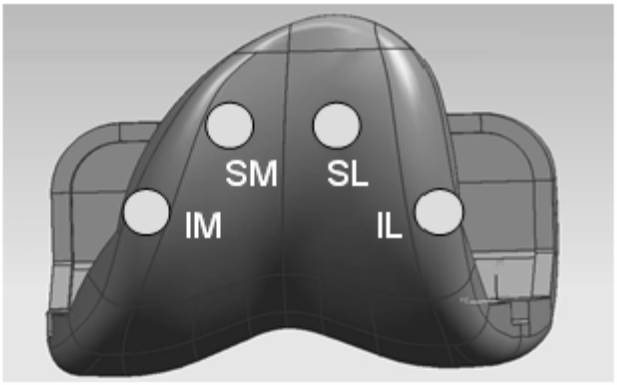

SM = Superior Medial

SL = Superior Lateral

IM = Inferior Medial

IL = Inferior Lateral

	SM	SL	IM	IL	Superior	Inferior	Pooled
N	5	7	8	8	12	16	28
BMAD (g/cm^3)	0.0476 ± 0.0198	0.0686 ± 0.0169	0.0666 ± 0.025	0.0836 ± 0.0366	0.0599 ± 0.0204	0.0751 ± 0.0316	0.0686 ± 0.028
E (MPa)	131 ± 52	208 ± 73	390 ± 183	664 ± 510	* 176 ± 74	* 527 ± 396	376 ± 347
σ_{yield} (MPa)	1.43 ± 0.58	2.40 ± 0.91	3.41 ± 1.43	4.61 ± 2.88	* 2.00 ± 0.91	* 4.01 ± 2.28	3.15 ± 2.06
$\sigma_{ultimate}$ (MPa)	1.47 ± 0.59	2.47 ± 0.92	3.47 ± 1.45	4.70 ± 3.01	* 2.05 ± 0.92	* 4.09 ± 2.37	3.21 ± 2.13
ε_{yield} (%)	1.26 ± 0.19	1.35 ± 0.17	1.15 ± 0.23	0.977 ± 0.168	* 1.31 ± 0.17	* 1.07 ± 0.21	1.17 ± 0.23
$\varepsilon_{ultimate}$ (%)	1.54 ± 0.39	1.65 ± 0.29	1.08 ± 0.53	1.14 ± 0.36	* 1.61 ± 0.32	* 1.20 ± 0.33	1.37 ± 0.38

Figure 5: Mean and standard deviation of material properties for all four locations, superior and inferior locations, and the pooled data of the distal femur. The inferior location has a higher apparent modulus, yield stress and ultimate stress, but has a lower yield and ultimate strain than the superior location.

* = Superior and inferior locations are significantly different ($p < 0.05$) for apparent modulus, yield stress, ultimate stress, yield strain and ultimate strain.

Table 1: Power law relationships between mechanical properties and bone mineral apparent density for all locations. BMAD is in units of g/cm^3. 95% confidence intervals are included in parentheses.

NS = not significantly different from zero ($p > 0.05$)

* = Superior and Inferior locations are significantly different ($p < 0.05$).

		$y = A \times BMAD^b$			
Property	Location	A	p	b	p
E (MPa)	Superior*	1920 (592, 6230)	< 0.0005	0.857 (0.453, 1.26)	0.001
	Inferior*	16100 (2450, 105000)	< 0.0005	1.37 (0.67, 2.07)	0.001
	Pooled	12100 (2880, 50600)	< 0.0005	1.37 (0.85, 1.88)	< 0.0005
σ_{yield} (MPa)	Superior*	20.2 (4.9, 84.0)	0.001	0.835 (0.345, 1.32)	0.003
	Inferior*	87.6 (20.5, 375)	< 0.0005	1.22 (0.68, 1.76)	< 0.0005
	Pooled	67.0 (22.9, 196)	< 0.0005	1.18 (0.79, 1.56)	< 0.0005
$\sigma_{ultimate}$ (MPa)	Superior*	19.7 (4.7, 83.0)	0.001	0.816 (0.323, 1.31)	0.004
	Inferior*	91.3 (21.7, 384)	< 0.0005	1.23 (0.69, 1.76)	< 0.0005
	Pooled	67.2 (23.2, 195)	< 0.0005	1.17 (0.79, 1.55)	< 0.0005
ε_{yield} (% strain)	Superior*	1.35 (0.71, 2.54)	< 0.0005	NS	0.9
	Inferior*	0.750 (0.33, 1.70)	< 0.0005	NS	0.4
	Pooled	0.798 (0.46, 1.40)	< 0.0005	NS	0.2
$\varepsilon_{ultimate}$ (% strain)	Superior*	1.67 (0.64, 4.37)	< 0.0005	NS	0.9
	Inferior*	1.24 (0.37, 4.10)	< 0.0005	NS	0.9
	Pooled	1.05 (0.46, 2.40)	< 0.0005	NS	0.6

Table 2: Linear relationships between mechanical properties and bone mineral apparent density for all locations. BMAD is in units of g/cm^3. 95% confidence intervals are included in parentheses.

NS = not significantly different from zero ($p > 0.05$)

* = Superior and Inferior locations are significantly different ($p < 0.05$).

		y = c x BMAD + d			
Property	Location	c	p	d	p
E (MPa)	Superior*	3070 (1720, 4410)	< 0.0005	NS	0.8
	Inferior*	9210 (4320, 14100)	0.001	NS	0.4
	Pooled	8920 (5430, 12400)	< 0.0005	NS	0.07
σ_{yield} (MPa)	Superior*	34.3 (14.3, 54.2)	0.003	NS	0.9
	Inferior*	60.5 (38.0, 83.0)	< 0.0005	NS	0.5
	Pooled	60.2 (43.1, 77.4)	< 0.0005	NS	0.1
$\sigma_{ultimate}$ (MPa)	Superior*	34.3 (13.5, 55.1)	0.004	NS	0.997
	Inferior*	63.1 (39.7, 86.5)	< 0.0005	NS	0.5
	Pooled	62.2 (44.5, 79.8)	< 0.0005	NS	0.1
ε_{yield} (% strain)	Superior*	NS	0.98	1.31 (0.94, 1.68)	< 0.0005
	Inferior*	NS	0.4	1.17 (0.87, 1.47)	< 0.0005
	Pooled	NS	0.2	1.32 (1.09, 1.56)	< 0.0005
$\varepsilon_{ultimate}$ (% strain)	Superior*	NS	0.98	1.60 (0.90, 2.30)	< 0.0005
	Inferior*	NS	0.6	1.09 (0.60, 1.57)	< 0.0005
	Pooled	NS	0.7	1.44 (1.03, 1.84)	< 0.0005

4. Discussion

The goal of this study was to investigate the relationship between BMAD and AP mechanical properties of cancellous bone in the human distal femur. The AP properties are important in the press-fit of the femoral knee component in a TKA operation and have not previously been established by mechanical testing at this anatomic location. The results of this study show significant relationships between BMAD and the AP apparent modulus of elasticity, yield stress and strain, and ultimate stress and strain. The results of the current study showed that each of the mechanical properties was dependent on SI coring location within the distal femur.

The first difference between this study and previous studies is that in the current study mechanical properties were determined by mechanical testing in the AP direction (Rho et al., 1995, determined AP properties using ultrasound). Others have determined properties along the axis of principal trabeculae

orientation or in the direction of the long axis of the bone, as was previously mentioned. Secondly, this study also measured the properties in the human distal femur. This anatomical location has not been researched as frequently as the proximal femur, tibia, and vertebrae regions. Finally, this study measured density as BMAD as opposed to apparent density or QCT. The difference in the type of density measurement, along with the difference in anatomical location, contributed to different density ranges between the current study and previous work.

The relationships between apparent modulus of elasticity and BMAD were different in the superior and inferior regions. The power coefficients were 0.857, 1.37, and 1.37 for the superior, inferior, and pooled data, respectively. In other literature, the power law between apparent modulus of elasticity and apparent density was found to have a squared (Rice et al., 1988) or cubic (Carter and Hayes, 1977) relationship. Morgan et al. (2003) found that modulus–density relationships differ between anatomic locations. They found power law modulus–density relationships with the power coefficient ranging from 1.49 to 1.93. Kopperdahl et al. (2002) found power law QCT modulus and QCT-yield stress power law coefficients of 1.05 and 1.39 in the spine. It is difficult to compare the current results with the results from past studies because apparent or QCT density has been used in past studies and BMAD was used here. To the authors' knowledge, there has been no study relating QCT and BMAD in cancellous bone.

The results of the current study showed significant linear relationships ($p < 0.0005$) between both yield stress ($R^2 = 0.91, 0.63, 0.71$ for superior, inferior, and pooled, respectively) versus apparent modulus and ultimate stress versus apparent modulus ($R^2 = 0.90, 0.61, 0.70$). These results were consistent with previous studies by Goldstein et al. (1983) ($R^2 = 0.89$) who used ultimate stress and Keaveny et al. (1994b) ($R^2 = 0.85$) who used yield stress.

The results of the current study showed that in the power law model, the multipliers were significant (po0.0005) for each of the yield and ultimate strain–BMAD relationships (superior, inferior, and pooled) while the power coefficients were not. The fact that the power coefficients were not significantly different from zero makes the power law equations independent of BMAD. It was found that only the constants in the linear relationship between both yield strain and BMAD and ultimate strain and BMAD were significant (po0.0005) for each of the relationships (superior, inferior, and pooled). The multipliers were not significant in any of the relationships. Thus in both the linear and power law models, the strains were independent of BMAD. Keaveny et al. (1994b) also found no significant relationship between both yield and ultimate strain and QCT density. Kopperdahl and Keaveny (1998) found that on-axis yield strain had a weak but significant correlation with apparent density, but ultimate strain did not. Kopperdahl et al. (2002) found that on-axis yield strains had a weak but significant correlation with QCT density.

The primary reason for the difference between the modulus and stress values in the superior and inferior is the orientation of the trabecular architecture. The principal direction of the trabecular architecture and the approximate AP coring orientation is shown in Figs. 6 and 7 (Hall, 1966).

Figure 6 shows the distal femur architecture in transverse planes. The trabecular architecture is oriented more along the general core axis in the inferior locations (Figure 6b) than Q3 the superior locations (Figure 6a) in the transverse plane. Figure 7 shows the distal femur architecture in sagittal planes. The principal direction of the trabecular architecture within the general core axis is less clear in this plane than in the transverse plane. In each image (Figure 7a–d), the trabecular orientation appears to be perpendicular to the general core axis through much of the length of the core. Within some of the cores there are shorter regions where the orientation is about 45° to the general core axis (Figure 7b–d). The difference in orientation between the superior and inferior locations is not as conclusive in the sagittal plane as it is in the transverse plane.

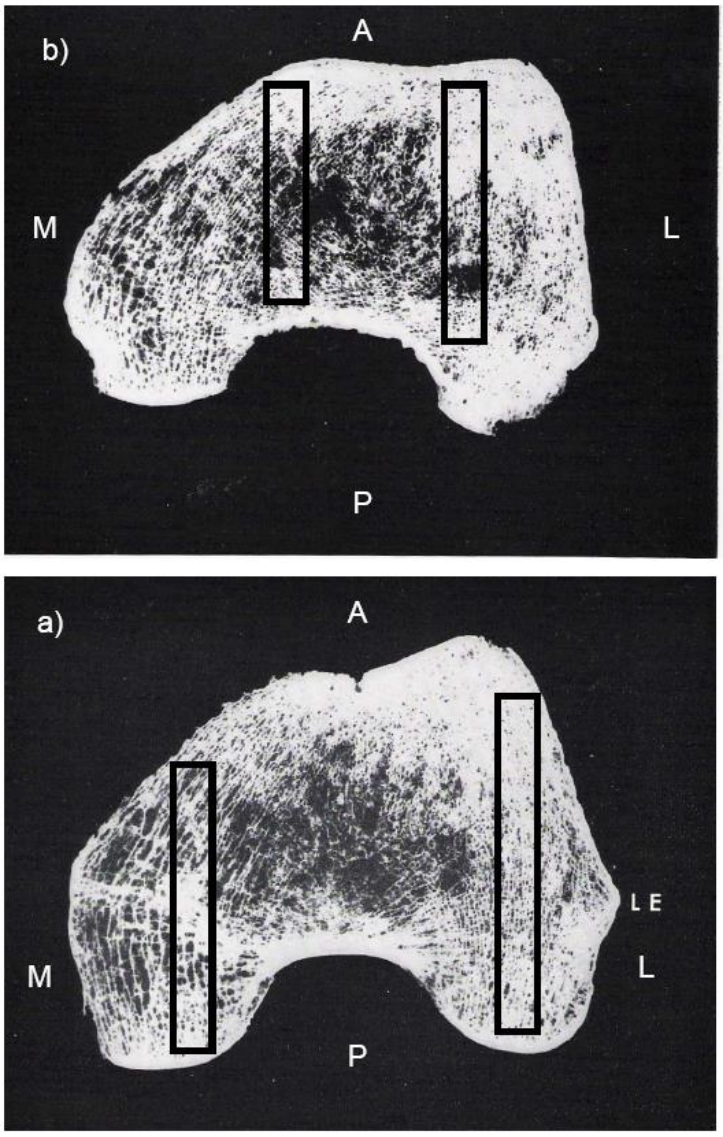

Figure 6: Transverse sections of the distal femur showing the trabecular architecture. Approximate coring locations are included. a) Superior coring locations, b) Inferior coring locations. Original images used with permission from Michael C. Hall, The Architecture of Bone, 1966. Courtesy of Charles C Thomas Publisher, Ltd., Springfield, Illinois. Images modified to emphasize region of interest.

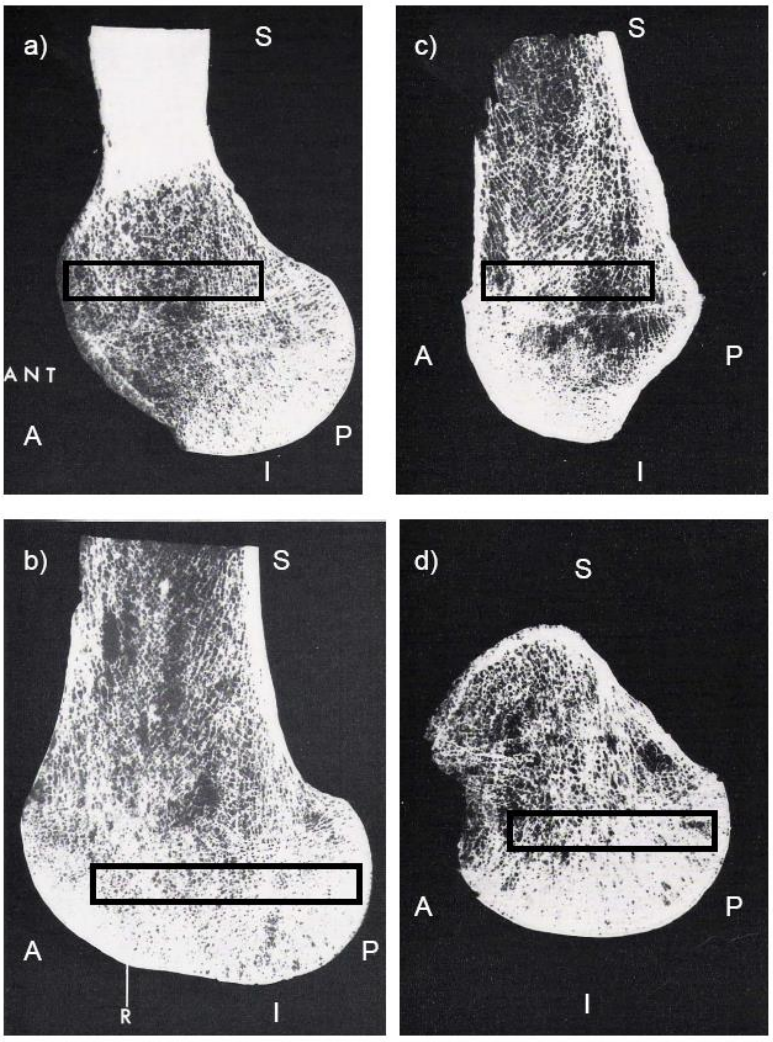

Figure 7: Sagittal sections of the distal femur showing the trabecular architecture. Approximate coring locations are included. a) Superior medial coring locations, b) Inferior medial coring locations, c) Superior lateral coring locations d) Inferior lateral coring locations. Original images used with permission from Michael C. Hall, The Architecture of Bone, 1966. Courtesy of Charles C Thomas Publisher, Ltd., Springfield, Illinois. Images modified to emphasize region of interest.

The differences in the orientation of the cores relative to the bone architecture caused a higher rate of increase with density for the modulus and stress values of the inferior than the superior cores. For the same density of bone, an AP inferior core was generally more aligned to the principal axis of the trabecular architecture than a superior core. The effect of orientation also led to a higher variance in the modulus–density relationships. Since the inferior cores were more closely aligned to the trabecular orientation, a variance in the orientation of the AP core with respect to the trabecular orientation was expected to cause higher variability in the data compared to the superior cores. The coefficients of determination for the modulus–-density relationship of the inferior cores were therefore lower than those of the superior cores. The effect of microstructure on the yield and ultimate strains is not well understood and may be an area of future study.

As mentioned, each of the five AP property–density relationships was significantly different at the superior and inferior locations. Properties have previously been shown to vary within anatomic location (Goldstein

et al., 1983). The variation found here was likely due to the trabecular architecture variance within the distal femur. It may not be the case that the properties would vary within the distal femur if the bone cores were tested on-axis. It is also expected that bone pathologies would affect the architecture in a manner different from those of a healthy bone; therefore, property–density relationships for pathological bone could only be determined by testing pathological bone.

The primary significance of this study is that the property–density relationship of the distal femoral bone varies between superior and inferior locations. This is important for the press-fit fixation of the bone–implant interface because the anterior shield is in contact with the superior region and the posterior condyles are in contact with the inferior region. The results presented in this paper have possible applications for implant design and preoperative assessment using clinical tools to estimate whole bone strength and modulus in the distal femur. Additionally, these property–density relationships will be critical to the assignment of mechanical properties in FE models for further investigation of the press-fit interface of femoral knee components. Quantifying the loads of this interface will provide a better understanding of the mechanical interaction between the implant and the bone. Quantifying the loads of the bone–prosthesis interface is an important first step in understanding the complex mechanism of component loosening, the primary cause of knee femoral component failure.

5. Conflict of interest

Dr. Mason is an employee of Zimmer, Inc., manufacturer of the NexGen implant system.

6. Acknowledgments

T. Burgers gratefully acknowledges the support of Zimmer, Inc. for this study. The authors also acknowledge Geoff Piller for his help in processing the data.

7. References

Carter, D.R., Hayes, W.C., 1977. The compressive behavior of bone as a two-phase porous structure. Journal of Bone and Joint Surgery— American 7, 954–962.

Carter, D.R., Bouxsein, M.L., Marcus, R., 1992. New approaches for interpreting projected bone densitometry data. Journal of Bone and Mineral Research 2, 137–145.

Ciarelli, M.J., Goldstein, S.A., Kuhn, J.L., Cody, D.D., Brown, M.B., 1991. Evaluation of orthogonal mechanical properties and density of human trabecular bone from the major metaphyseal regions with materials testing and computed tomography. Journal of Orthopaedic Research 5, 674–682.

Cody, D.D., Gross, G.J., Hou, F.J., Spencer, H.J., Goldstein, S.A., Fyhrie, D.P., 1999. Femoral strength is better predicted by finite element models than QCT and DXA. Journal of Biomechanics 10, 1013–1020.

Du, C., Ma, H., Ruo, M., Zhang, Z., Yu, X., Zeng, Y., 2006. An experimental study on the biomechanical properties of the cancellous bones of distal femur. Bio-Medical Materials and Engineering 3, 215–222.

Esses, S.I., Lotz, J.C., Hayes, W.C., 1989. Biomechanical properties of the proximal femur determined in vitro by single-energy quantitative computed tomography. Journal of Bone and Mineral Research 5, 715–722.

Fehring, T.K., Griffin, W.L., 1998. Revision of failed cementless total knee implants with cement. Clinical Orthopaedics and Related Research 356, 34–38.

Fehring, T.K., McAvoy, G., 1996. Fluoroscopic evaluation of the painful total knee arthroplasty. Clinical Orthopaedics and Related Research 331, 226–233.

Fehring, T.K., Odum, S., Griffin, W.L., Mason, J.B., Nadaud, M., 2001. Early failures in total knee arthroplasty. Clinical Orthopaedics and Related Research 392, 315–318.

Gibson, L.J., Ashby, M.F., 1997. Cellular Solids—Structure and Properties, second ed. Press Syndicate of the University of Cambridge, Cambridge, UK, pp. 183–192.

Goldstein, S.A., Wilson, D.L., Sonstegard, D.A., Matthews, L.S., 1983. The mechanical properties of human tibial trabecular bone as a function of metaphyseal location. Journal of Biomechanics 12, 965–969.

Hall, M.C., 1966. The Architecture of Bone. Charles C. Thomas, Springfield, IL, pp. 183–193.

Huiskes, R., Chao, E.Y., 1983. A survey of finite element analysis in orthopedic biomechanics: the first decade. Journal of Biomechanics 6, 385–409.

Hvid, I., Bentzen, S.M., Linde, F., Mosekilde, L., Pongsoipetch, B., 1989. X-ray quantitative computed tomography: the relations to physical properties of proximal tibial trabecular bone specimens. Journal of Biomechanics 8–9, 837–844.

Insall, J.N., Hood, R.W., Flawn, L.B., Sullivan, D.J., 1983. The total condylar knee prosthesis in gonarthrosis. A five to nine-year follow-up of the first one hundred consecutive replacements. Journal of Bone and Joint Surgery—American 5, 619–628.

Keaveny, T.M., Guo, X.E., Wachtel, E.F., McMahon, T.A., Hayes, W.C., 1994a. Trabecular bone exhibits fully linear elastic behavior and yields at low strains. Journal of Biomechanics 9, 1127–1136.

Keaveny, T.M., Wachtel, E.F., Ford, C.M., Hayes, W.C., 1994b. Differences between the tensile and compressive strengths of bovine tibial trabecular bone depend on modulus. Journal of Biomechanics 27, 1137–1146.

Keaveny, T.M., Pinilla, T.P., Crawford, R.P., Kopperdahl, D.L., Lou, A., 1997. Systematic and random errors in compression testing of trabecular bone. Journal of Orthopaedic Research 1, 101–110.

Keyak, J.H., Meagher, J.M., Skinner, H.B., Mote Jr., C.D., 1990. Automated three-dimensional finite element modelling of bone: a new method. Journal of Biomedical Engineering 5, 389–397.

Kopperdahl, D.L., Keaveny, T.M., 1998. Yield strain behavior of trabecular bone. Journal of Biomechanics 7, 601–608.

Kopperdahl, D.L., Morgan, E.F., Keaveny, T.M., 2002. Quantitative computed tomography estimates of the mechanical properties of human vertebral trabecular bone. Journal of Orthopaedic Research 4, 801–805.

Lotz, J.C., Gerhart, T.N., Hayes, W.C., 1990. Mechanical properties of trabecular bone from the proximal femur: a quantitative CT study. Journal of Computer Assisted Tomography 1, 107–114.

McBroom, R.J., Hayes, W.C., Edwards, W.T., Goldberg, R.P., White 3rd, A.A., 1985. Prediction of vertebral body compressive fracture using quantitative computed tomography. Journal of Bone and Joint Surgery—American 8, 1206–1214.

Morgan, E.F., Yeh, O.C., Chang, W.C., Keaveny, T.M., 2001. Nonlinear behavior of trabecular bone at small strains. Journal of Biomechanical Engineering 1, 1–9.

Morgan, E.F., Bayraktar, H.H., Keaveny, T.M., 2003. Trabecular bone modulus–density relationships depend on anatomic site. Journal of Biomechanics 7, 897–904.

Nielsen, S.P., 2000. The fallacy of BMD: a critical review of the diagnostic use of dual X-ray absorptiometry. Clinical Rheumatology 3, 174–183.

Perillo-Marcone, A., Ryd, L., Johnsson, K., Taylor, M., 2004. A combined RSA and FE study of the implanted proximal tibia: correlation of the post-operative mechanical environment with implant migration. Journal of Biomechanics 8, 1205–1213.

Pilliar, R.M., 2005. Cementless implant fixation—toward improved reliability. Orthopedic Clinics of North America 1, 113–119.

Reckling, F.W., Asher, M.A., Dillon, W.L., 1977. A longitudinal study of the radiolucent line at the bone–cement interface following total joint replacement procedures. Journal of Bone and Joint Surgery—American 3, 355–358.

Rho, J.Y., Hobatho, M.C., Ashman, R.B., 1995. Relations of mechanical properties to density and CT numbers in human bone. Medical Engineering and Physics 5, 347–355.

Rice, J.C., Cowin, S.C., Bowman, J.A., 1988. On the dependence of the elasticity and strength of cancellous bone on apparent density. Journal of Biomechanics 2, 155–168.

Sharkey, P.F., Hozack, W.J., Rothman, R.H., Shastri, S., Jacoby, S.M., 2002. Insall award paper. Why are total knee arthroplasties failing today? Clinical Orthopaedics and Related Research 404, 7–13.

Shultz, T.R., Blaha, J.D., Gruen, T.A., Norman, T.L., 2006. Cortical bone viscoelasticity and fixation strength of press-fit femoral stems: finite element model. Journal of Biomechanical Engineering 1, 7–12.

Taylor, W.R., Roland, E., Ploeg, H., Hertig, D., Klabunde, R., Warner, M.D., Hobatho, M.C., Rakotomanana, L., Clift, S.E., 2002. Determination of orthotropic bone elastic constants using FEA and model analysis, Journal of Biomechanics 767–773.

Turner, C.H., Cowin, S.C., 1988. Errors induced by off-axis measurement of the elastic properties of bone. Journal of Biomechanical Engineering 3, 213–215.

Verdonschot, N.J., Huiskes, R., Freeman, M.A., 1993. Pre-clinical testing of hip prosthetic designs: a comparison of finite element calculations and laboratory tests. Proceedings of the Institution of Mechanical Engineers H 3, 149–154.

Zysset, P.K., Goulet, R.W., Hollister, S.J., 1998. A global relationship between trabecular bone morphology and homogenized elastic properties. Journal of Biomechanical Engineering 5, 640–646.